https://doi.org/10.5194/angeo-2021-65
Preprint. Discussion started: 10 November 2021

Annales Geophysicae Discussions

Propagating characteristics of mesospheric gravity waves observed by an OI 557.7 nm airglow all-sky camera at Mt. Bohyun (36.2°N, 128.9°E)

Jun-Young Hwang[1], Young-Sook Lee[1], Yong Ha Kim[1], Hosik Kam[2], Young-Sil Kwak[2,3], Tae-Yong Yang[2]

[1]Department of Astronomy and Space Science, Chungnam National University, Daejeon, South Korea.

[2]Korea Astronomy and Space Science Institute, Daejeon, South Korea.

[3]Department of Astronomy and Space Science, University of Science and Technology, Daejeon, South Korea.

Corresponding author: Young-Sook Lee yslee0923@cnu.ac.kr

Abstract

We analyzed all-sky camera images observed at Mt. Bohyun observatory (36.2°N, 128.9°E) for the period of 2017 - 2019. The image data were acquired with a narrow band filter centered at 557.7 nm for the OI airglow emission at ~96 km altitude. The total of 150 wave events were identified in the images of 144 clear nights. The interquartile ranges of wavelength, phase speed, and periods of the identified waves are 20.5 - 35.5 km, 27.4 - 45.0 m/s and 10.8 -13.7 min with the median values of 27.8 km, 36.3 m/s and 11.7 min, respectively. The summer and spring bias of propagation directions of northeast- and northward, respectively, can be interpreted as the effect of filtering by the prevailing winds in the lower atmosphere. In winter the subdominant northwestward waves may be observed due to nullified filtering effect by small northward background wind or secondary waves generated in the upper atmosphere. Intrinsic phase speeds and periods of the waves were also derived by using the wind data simultaneously observed by a nearly co-located meteor radar. The nature of vertical propagation was evaluated in each season. The majority of observed waves are found to be freely propagating, and thus can be attributed to wave sources in the lower atmosphere.

Keywords: atmospheric gravity wave, horizontal and vertical propagation, Doppler effect, filtering effect, wave ducting

1.Introduction

Short-period atmospheric gravity waves (<100 min) are well known for playing an important role in carrying energy and momentum from the lower atmosphere, upward propagating and depositing them into the mesosphere and lower thermosphere (MLT) region (Lindzen, 1981; Fritts and Alexander, 2003). In the mid- and high-latitude MLT region the transported energy and momentum are deposited through the breaking and dissipating processes of gravity waves, and affect significantly the zonal flow in both hemispheres, which in turn causes the pole-to-pole circulation resulting in the cold and warm mesosphere in summer and winter, respectively (Lindzen, 1981; Fritts and Vincent, 1987; Fritts and Alexander, 2003; Becker, 2012). Atmospheric gravity waves are generated by a number of causes or mechanisms, such as mountainous terrain, convective activity triggered by severe weather phenomena, wind shear, and areas with high baroclinic instability (Fritts and Alexander, 2003).

The characteristics of short-period gravity waves have been studied by the observation of airglow emission in the MLT region. Airglow imaging technique has been developed to observe gravity waves directly by using a wide-field or all-sky lens with a highly sensitive cooled charge-coupled device (CCD) detector. The observation using an all-sky camera has an advantage of being able to derive various parameters of gravity waves through series of processing in time and spatial domains. Time series of all-sky airglow images can be converted into series of 2-dimensional image arrays that can be analyzed objectively to obtain the horizontal wavelength, propagation phase speed and period of the wave (Taylor et al., 1993).

An all-sky imager had been deployed at Bohyun observatory (BHO, 36.2°N, 128.9° E) to observe various airglows, including OH Meinel 720-910 nm, O_2 atmospheric band near 865.7 nm, OI 630 nm and OI 557.7 nm in the pilot period of 2002 - 2005. Later, the all-sky camera at BHO focused on the OI 557.7 airglow observation because the throughput of the OI 557.7 filter is far more efficient than other filters. The previous studies with the all-sky observation at BHO have reported seasonal variation of wave parameters and horizontal propagation directions (Kim et al., 2010; Yang et al., 2015).

https://doi.org/10.5194/angeo-2021-65
Preprint. Discussion started: 10 November 2021

Annales Geophysicae Discussions

The characteristics of vertical propagation of gravity waves can be determined by the relationship between the horizontal phase speed of gravity waves and the background wind field, and vertical temperature profile. The nature of vertical propagation can be classified into critical-level filtering, ducting, and freely propagating modes. Critical-level filtering effect is caused when the horizontally propagating wave meets with the same vector of background wind, and the wave would be absorbed or reflected out (Kim and Chun, 2010; Heale and Snively, 2015). The wave that is reflected from the upper and (or) lower altitude regions can be (partially) ducted (Fritts and Alexander, 2003). The wave ducting can occur when the wave propagates against background wind field, at which background wind profile has a local maximum, called Doppler ducting (Chimonas and Hines, 1986; Isler, 1997; Nappo, 2002; Suzuki et al., 2013). In addition, large vertical changes of background winds such as wind shear or curvature wind can provide a favorable condition to cause Doppler ducting (e.g., Chimonas and Hines,1986; Isler et al., 1997). The ducted wave can horizontally propagate much longer distance than freely propagating waves (Isler et al., 1997; Hecht et al., 2001, 2004; Pautet et al., 2005). In freely propagating mode, horizontally propagating waves can be Doppler shifted by opposing or forwarding background wind. Therefore, the background wind can play a crucial role in evaluating the nature of both vertical and horizontal propagation of gravity waves. Fortunately, we were able to take advantage of the background wind measurements around the OI airglow layer by a meteor radar at Gyeryong nearby BHO.

This study reports the characteristics of the apparent and intrinsic parameters of observed gravity waves by using the all-sky imaging data for the period of 2017 – 2019 along with the mesospheric wind data that were simultaneously observed by a meteor radar. The intrinsic parameters of gravity waves allow to understand the relation between the observed wave directions and the background winds as well as the nature of vertical propagation at mid-latitude mesosphere around the east Asia.

2. Observational and model data

We analyze OI 557.7 airglow images observed by the all-sky camera at BHO from April 2017 through December 2019. Images of the total 144 nights were used in the analysis by excluding the cases of cloudy and moon-lit nights and equipment malfunction. The all-sky camera at BHO is an ultra-high speed (f/0.95) 3-inch camera composed of a fisheye lens with a viewing angle of 180°, telecentric lens to adjust airglow emission light path for parallel incident to filter, a 6-position filter wheel installed with two narrowband filters (OI-557.7, OI-630.0), and a 1024×1025 CCD detector. The detail description of the all-sky camera at BHO has been given in Yang et al. (2015). The images with the OI 557.7 filter were obtained continuously at intervals of 5 minute with an exposure time of 90-150 seconds and a spatial resolution of 500 km radial region. The OI-630.0 nm filter was not used in this period of observation.

A very-high frequency (VHF) meteor radar system has been operating at Gyeryong station (36.2°N, 127.1°E), since November, 2017. The Enhanced Meteor Detection Radar (EMDR) system (supplied by ATRAD Pty Ltd) is an interferometric radar consisting of five channels. The system is operated with specifications of a transmitter peak power of 24 kW, duty cycle of 8.4 % from 2017/11-2018/05 and 4.2 % from 2018/05 to the present. The meteor radar provides meridional and zonal winds at 2 km bin in the 80 – 100 km altitude range every hour. The wind data were utilized when the intrinsic wave parameters and vertical propagation were examined. In addition, the temperature information between 80 and 100 km was adopted from the NRLMSIS2.0 model when the Brunt- Väisälä frequency was computed to evaluate the vertical wavelengths of gravity waves.

3. Data processing for acquiring wave parameters

The procedure to acquire the wave parameters can be separated into two steps: pre-processing of all-sky camera images and the image processing with 2D image. The pre-processing includes image selection of clear nights (see Figure 1a), star removing, transforming fisheye lens image into the horizontal plane image (500 km×500 km, see Figure 1b) at the OI 557.7 airglow altitude of 96 km. The details of pre-processing method are provided in Kam (2016).

Time series of pre-processed images were first converted into time-difference images (Figure 2a), from which large-scale modulation was removed by applying 2D bandpass filtering (Figure 2b). The time-difference (TD) image is obtained from two consecutive images (see Figure 1b) by subtracting from one to another. We then applied 2D Fast Fourier Transformation

https://doi.org/10.5194/angeo-2021-65
Preprint. Discussion started: 10 November 2021

Annales Geophysicae Discussions

(FFT) to derive wave parameters of quasi-monochromatic waves from the series of TD images (Tang et al, 2005).

The 2D FFT operation of two TD images produces 2D spectrum arrays of J1 and J2, which can be cross-correlated as in Equation 1 to derive a phase difference $(\phi_1 - \phi_2)$ of the wave

$$\mathrm{f}(\mathrm{k_x}, k_y) = J_1(k_x, k_y) J_2^*(k_x, k_y) = R_1 R_2 \exp(i\,(\phi_1 - \phi_2)), \qquad (1)$$

where $\mathrm{k_x}$ and k_y are zonal and meridional wave numbers, respectively. The value of $|R_1 R_2|^2$ derived from $|\mathrm{f}(\mathrm{k_x}, k_y)|^2$ represents the magnitude of the wave. The dominant wave was chosen at the maximum magnitude, whose $\mathrm{k_x}$ and k_y provide the wavelengths of the dominant wave. Along with the time difference and the wavelength information, the phase difference allows to determine the observed phase speed of the dominant wave.

4. Characteristics of observed waves at Mt. Bohyun

The total of 150 wave events were identified from the all-sky image data for 3 years (2017-2019). For these wave events, horizontal wavelength, observed phase speed, observed period, and propagation direction of the dominant wave are derived and their distributions are plotted as in Figure 3. The interquartile range (IQR) of wavelength is spanned from 20.5-35.5 km with a median value of 27.8 km; the observed phase speed IQR is from 27.4-45.0 m/s with a median of 36.3 m/s, and the period IQR is from 10.8-13.7 with a median of 11.7 min. In addition, the predominant propagating directions are north (44%) and northeast (33%). The characteristics of these wave parameters were similar to the results of Kim et al. (2010).

In order to compare consistently the results of Takeo et al. (2017), which reported the similar observation in the east Asia, we divided seasons in the same way: from February 21 - April 19 (2 months) for spring, from April 20 - August 20 (4 months) for summer, from August 21-October 20 (2 months) for fall, and from October 21 - February 20 (4 months) for winter. Seasonal wave propagation vectors and their occurrences are shown in Figures 4a-d. The seasonal occurrences for observed (yellow) horizontal wavelength, observed phase speed, and observed period, and intrinsic (green) phase speed and period are shown in Figure 5. The median values of the parameters for each season are summarized in Table 1. In spring, the propagation primarily to the northeast and next the north takes up 35% and 24% out of 29 cases, respectively, as shown in Figure 4a. In summer, propagation directions to the north (50%) and northeast (35%) are dominant (Figure 4b). In fall, the wave seems to propagate all-direction without preference (Figure 4c). The fall season contains particularly small number of wave events due to equipment problem and poor weather. In winter, the propagation directions seem to be grouped into the south (27%), northwestward (23%) and southwest (16%) (see Figure 4d). In terms of the median values, the observed phase speed in winter is particularly slower than other seasons, whereas other parameters show little variation. Overall it is evident that in spring/summer, the northward and northeastward propagating gravity waves are dominant, whereas in winter the southward and northwestward propagations are dominant. The distinct seasonal properties of propagation direction can be attributed to the filtering effect by the background wind field during the gravity wave propagation from the lower atmosphere (e.g. Kim et al., 2010; Kim and Chun, 2010; Heale and Snively, 2015).

In order to confirm the filtering effect on the seasonal variation of observed propagation direction, we checked the horizontal winds of the MERRA, version 2 (MERRA-2): MERRA-2 is an atmospheric reanalysis model created by NASA's Global Modeling and Assimilation Office (GMAO, https://gmao.gsfc.nasa.gov/reanalysis/MERRA-2/data_access/). MERRA-2 reanalysis data are available for 0-80 km altitudes and 0.5°×0.625° latitude and longitude resolutions. As well known, in the spring/summer the westward wind is dominant in the middle atmosphere, whereas in the fall/winter the eastward wind is dominant (not shown). In addition, MR-observed annual variations of zonal and meridional winds for years of 2017-2020 are available for 80-100 km (Kam et al., 2021). Here, prevailing winds in spring and summer are observed in westward and southward at 80-100 km, seemingly continued from 10-80 km altitudes, while in winter eastward winds are maintained in 80-100 km, but small northward winds (<~10 m/s) less than 90 km turn to the southward above 90 km. It is reasonable to suggest that westward waves in spring and summer may have been filtered out by the westward wind, and thus are hardly observed. The southward wind in spring/summer may also have filtered out the southward waves, which is consistent with our observation. Furthermore, in summer it is well known that the convective system of typhoons or tropical cyclones can be significant

https://doi.org/10.5194/angeo-2021-65
Preprint. Discussion started: 10 November 2021

sources of gravity waves in the middle latitude. The typhoon-generated gravity waves in the south of the Korean peninsula can propagate any directions, but the westward propagating waves might be filtered out in the stratosphere by the prevalent westward wind. Therefore, northward or northeastward propagating waves are obviously observed in Korea. The details about typhoon-generated gravity waves can be referred to Kim and Chun (2010). In winter, it is expected that eastward/northward waves be well filtered out by prevailing the eastward/northward winds. However, although our observation shows southward/westward preferential directions (see Figure 4d), northwestward waves are also subdominant. The significant northward component of the wave direction may not be blocked by filtering effect. In the meanwhile, it seems to survive on upward propagation up to 96 km due to the small velocity (<10 m/s) of northward mean field. Otherwise, the northwestward wave in winter may be interpreted as secondary waves or waves generated in the upper mesosphere.

The previous studies for mid-latitude gravity waves have reported in the majority the dominance of eastward and northward propagations during summer (Taylor et al., 1993; Nakamura et al., 1999; Walterscheid et al., 1999; Hecht et al., 2001; Ejiri et al., 2003; Tang et al., 2005). Observations at BHO have confirmed the similar tendency of propagation in summer (Kim et al, 2010; Yang et al, 2015). The summer bias of wave propagation can be distinctly due to the critical level filtering by the prevailing zonal and meridional winds in the lower atmosphere. However, the tendency of wave propagation also likely shows different patterns according to localized sources. For example, in spring for Shigaraki (34.9°N, 136.1°E) Takeo et al. (2017) observed using the OI 557.7 nm filter the dominant southwestward propagation in addition to the northeastward that is similar to our results in Figure 4a. In winter, the southward (equatorward) propagation was dominant in several studies although less than in summer (Hecht et al., 2001; Ejiri et al., 2003; Tang et al., 2005). Both Ejiri et al. (2003) and Takeo et al. (2017) observed southward dominant propagation for Shigaraki in winter. Besides, Ejiri et al. (2003) found that winter preferential propagation may vary with latitudes because both southward and poleward dominant propagations in both OH and OI observations were observed at Rikubetsu (43.6°N), a relatively high latitude site.

https://doi.org/10.5194/angeo-2021-65
Preprint. Discussion started: 10 November 2021

5. Characteristics of intrinsic gravity wave parameters

The OI 557.7 nm airglow layer has been reported to be peaked at 96 km with a thickness of ~7-9 km, including both disturbed and undisturbed conditions (Vargas et al., 2007). The waves with a vertical wavelength less than the airglow layer thickness may not be detected by an airglow imager due to sinusoidal cancellation (Nielsen et al., 2012; Vargas et al., 2007). The vertical wavelength of the observed wave can be derived from the simplified dispersion relation of gravity waves by neglecting a wind shear (e.g., Nappo, 2002), such as

$$m^2 \approx \frac{N^2}{c_i^2} - \frac{1}{4H_s^2} - k^2, \quad (2)$$

where N is the Brunt-Väisälä frequency, c_i the is intrinsic phase speed of gravity wave, and H_s is the scale height. The intrinsic phase speed, c_i, can be expressed as c-u, where c is the wave phase speed and u is the background wind speed in the wave propagating direction. The Brunt-Väisälä frequency is given as

$$N^2 = \frac{g}{T}\left(\frac{dT}{dz} + \frac{g}{C_p}\right), \quad (3)$$

where g is the gravity, 9.55 m/s^2, T is the atmospheric temperature, C_p is a specific heat capacity at constant pressure, adopted as 1005 $J/(K \cdot Kg)$ for a dry air (Brasseur and Solomon, 2005). H_s is given with RT/g, where R is the gas constant of dry air, 287 J/kg/K.

The intrinsic phase speeds of waves were computed by utilizing the wind at 96 km simultaneously measured by the Gyeryong meteor radar. The intrinsic period is calculated by λ_h/c_i, where λ_h is the observed horizontal wavelength. The IQR of intrinsic phase speed of gravity waves in spring is spanned from 15.7-67.3 m/s with a median value of 40.5 m/s, and the IQR of intrinsic period is from 6.3- 21.8 min with a median of 11.5 min. In summer the corresponding IQR values are 28.2-64.6 m/s with a median of 48.3 m/s, and 6.4 – 21.6 min with a median of 11.5 min; in winter, the IQR values are 10.1 – 65.9 m/s with a median of 32.9 m/s, and 7.9 – 19.9 min with a median of 11.7 min. It is noted that the intrinsic speeds for spring and summer are larger than the observed ones (see Figure 5), implying that the majority of waves occurred in the opposite direction to the background wind. The intrinsic speed has been

https://doi.org/10.5194/angeo-2021-65
Preprint. Discussion started: 10 November 2021

merely shifted to the larger observed by the Doppler effect. The results of intrinsic parameters exist in the typical values of gravity wave parameters such as intrinsic phase speeds of 30-100 m/s and intrinsic periods from 5-50 min (Taylor et al., 1997; Swenson et al., 2000; Hecht et al., 2001; Ejiri et al., 2003).

6. Characteristics of vertical propagation

The nature of vertical propagation can be evaluated by the vertical wave number squared, m^2 (Isler et al., 1997). If m^2 is greater than zero in the airglow-observed MLT region, the gravity wave is in freely propagating mode. If m^2 is less than zero, the wave is vertically evanescent, which indicates the wave motion only in the horizontal propagation. If the freely propagating region is bounded by evanescent regions below and above, the wave is in ducting mode. If it is bounded by one side evanescent region below or above, it is in partial ducting.

Based on the m^2 profile in 90-100 km centered at 96 km, the nature of vertical propagation can be classified for seasons, as summarized in Table 2. Freely propagating waves take up a maximum of 82% in summer and a minimum of 65% in spring. Ducted waves were 7% and 4% in summer and winter, respectively. Partial ducting takes up 28% and 20% for spring and winter, respectively. Evanescent waves (7%) are observed only in spring. The small percentage of evanescent waves may imply that the majority of the observed waves is not locally originated from, at least the altitude range of 90 – 100 km. The freely propagating waves show vertical wavelengths with a median value of 7.7 km and IQR ranged from 5.1-10.9 km. It should be noted that the temperature profile used in the computation of the Brunt-Väisälä frequency is the climatological one, not the real-time temperatures, which may result in the vertical wavelengths smaller than the airglow layer thickness.

The wave ducting can be primarily caused by the background wind, so called Doppler ducting, or primarily by a variation of Brunt-Väisälä frequency, so called thermal ducting. Since we use the climatologic temperature profile, we cannot identify the thermal ducting that requires real-time temperature measurements. On the other hand, Doppler ducting can be found rather confidently because we use the simultaneously measured wind profile. Doppler ducting is

https://doi.org/10.5194/angeo-2021-65
Preprint. Discussion started: 10 November 2021

favorable when the wind profile has a local maximum against the wave propagation (e.g., Chimonas and Hines, 1986; Isler, 1997; and Nappo, 2002).

Examples of vertical propagation nature appraised by m^2 are shown in Figures 6a-c, where the left panel presents the MR wind profile projected on the wave propagating direction, in which the negative means that the wind blows opposite to the wave propagation direction, and the right panel displays the m^2 profile.

In Figure 6a the gravity wave at a phase speed of c = 48.7 m/s was propagating northeastward (φ=52°) against the background wind at 90-100 km altitudes and the values of m^2 in the 90-100 km region are all positive, indicating the freely propagating nature.

Figure 6b shows an example of a Doppler ducted wave. Here the freely propagating region ($m^2 > 0$) at 90-98 km is encompassed with the negative values of m^2 above 98 km and below 90 km. The winds opposing the gravity wave propagation becomes large above 98 km and lower 90 km. Therefore, the wave can be trapped around 96 km vertically, but still propagate to the horizontal direction. Nielsen et al. (2012) noted that when jets occurred above and below the altitude region of freely propagating ($m^2 > 0$), the wave can be bounded by evanescent regions ($m^2 < 0$), causing Doppler ducting. Suzuki et al. (2013) observed an evidence of Doppler ducting under the large opposing winds: a northward propagating wave at a phase speed of 48 m/s lasting for ~5 hrs (11-17 UT) went through a strong southward wind, stretching over 16°x16° in latitude and longitude. For the ducted waves, it may be difficult to trace back the source of the waves.

Figure 6c presents an example of an evanescent wave, based on negative values of m^2 in the altitude range of 90- 97 km. The background wind is too fast in the opposing direction of the wave, prohibiting the vertical propagation. The evanescent waves may be generated in situ at the airglow layer, probably as secondary waves, not propagated from the lower atmosphere. The evanescent waves were very rare (less than 2%) in our analysis of the BHO images. The majority of observed waves are found to be freely propagating, and thus can be attributed to wave sources in the lower atmosphere.

https://doi.org/10.5194/angeo-2021-65
Preprint. Discussion started: 10 November 2021

7. Summary and conclusions

This study investigated the characteristics of horizontal and vertical propagation of atmospheric gravity waves observed at Mt. Bohyun observatory (BHO, 36.2°N, 128.9°E) for the period of 2017 - 2019. The data used are all-sky images of the OI 557.7 nm airglow layer (~96 km). Wind data in the 80 -100 km altitude range measured by a meteor radar at a nearly co-located site were utilized to derive intrinsic wave parameters and their vertical propagation nature.

The results of our analysis can be summarized as follows:

1. The total of 150 wave events were identified in the images of 144 clear nights. The interquartile ranges (IQR) of wavelength, observed phase speed, and observed periods of the identified waves are 20.5 - 35.5 km (with a median value of 27.8 km), 27.4 - 45.0 m/s (with a median value of 36.3 m/s) and 10.8 -13.7 min (with 11.7 min median value), respectively.
2. The observed waves propagate predominantly northeastward and northward in spring and summer, respectively. In winter the majority of waves propagate southward but the significant portion of waves northward. The seasonal preferential directions as in our observation have been reported by previous studies in east Asia, and interpreted as the consequence of the critical level filtering effect due to the prevailing wind in the lower atmosphere. The observed northwestward waves in winter may be caused by nullified filtering effect due to small background wind field, secondary waves or waves generated in the upper mesosphere.
3. Intrinsic phase speeds and periods of the waves were also derived by using the wind data simultaneously observed by a meteor radar. It is noted that the intrinsic speeds for spring and summer are larger than the observed ones because the majority of waves propagate in the opposite direction to the background wind.
4. The nature of vertical propagation was evaluated in each season. The freely propagating waves take up a maximum of 82% in summer and a minimum of 65% in spring. Ducted waves were 7% and 4% in summer and winter, respectively. Evanescent waves were 7% only in spring. The majority of observed waves are found to be freely propagating, and

https://doi.org/10.5194/angeo-2021-65
Preprint. Discussion started: 10 November 2021

thus can be attributed to wave sources in the lower atmosphere.

In conclusion, we find that both horizontal and vertical propagation characteristics of the observed waves at the OI 557.7 nm airglow layer are consistent with the notion that the majority of waves originated from the lower atmosphere and experienced the filtering effect by the prevailing winds in the intermediate atmosphere.

Data availability. We referred free reanalysis wind data from https://gmao.gsfc.nasa.gov/reanalysis/MERRA-2/dataaccess/, last access: August 10, 2020, for the mean wind field at altitudes of 0-80 km. We also used free model temperature data from https://map.nrl.navy.mil/map/pub/nrl/NRLMSIS/NRLMSIS2.0/, last access August 20, 2021 as an element in making our figures and table.

Supplement. Not applicable.

Author Contributions. Y. H. Kim and Y.-S. Lee conceived of the presented idea and the design of the study. J.-Y. Hwang and Y.-S. Lee manually gathered the data used. J.-Y. Hwang and Y.-S. Lee programmed for data analysis. The data analysis and interpretation of the results were done by Y. H. Kim and Y.-S. Lee. This paper was drafted and edited by Y.-S Lee and J.Y-. Hwang, and critically reviewed by T.-Y. Yang, H. Kam, Y.-S. Kwak and Y. H. Kim for content. Y.-S. Kwak and T.-Y. Yang took responsibility for overseeing the project. All authors have read and agreed to the published version of the manuscript.

Competing interests. The contact author has declared that neither they nor their co-authors have any competing interests.

https://doi.org/10.5194/angeo-2021-65
Preprint. Discussion started: 10 November 2021

Acknowledgements.

This research was supported by basic research funding from the Korea Astronomy and Space Science Institute (KASI) (KASI2021185005). We would like to acknowledge the Geospace Science & Technology Branch of U.S. Naval Research Laboratory (NRL) for providing the MSIS2.0 model data (https://map.nrl.navy.mil/map/pub/nrl/NRLMSIS/NRLMSIS2.0/), and NASA's Global Modeling and Assimilation Office for providing MERRA-2 atmospheric reanalysis model. We would like to thank the anonymous reviewers for the critical reviews that helped to improve this paper.

Review statement. This paper was edited by an editor (?) and reviewed by two anonymous referees.

https://doi.org/10.5194/angeo-2021-65
Preprint. Discussion started: 10 November 2021

References

Brasseur, G., and Solomon, S. (2005), *Aeronomy of the Middle Atmosphere: Chemistry and Physics of the Stratosphere and Mesosphere* (3rd ed.). Dordrecht: Springer.

Becker, E. (2012), Dynamical control of the middle atmosphere. *Space Sci. Rev., 168(1-4),* 238-314, doi:10.1007/s11214-011-9841-5

Chimonas, G., and C. O. Hines (1986), Doppler ducting of atmospheric gravity waves, *J. Geophys. Res., 91*, 1219–1230.

Ejiri, M., K. Shiokawa, T. Ogawa, K. Igarashi, T. Nakamura, and T. Tsuda (2003), Statistical study of short-period gravity waves in OH and OI nightglow images at two separated sites, *J. Geophys. Res., 108(D21),* 4679, doi:10.1029/2002JD002795.

Fritts, D. C., and R. A. Vincent (1987), Mesospheric momentum flux studies at Adelaide, Australia: Observations and a gravity wave/tidal interaction model, *J. Atmos. Sci., 44*, 605–619.

Fritts, D. C., and M. J. Alexander (2003), Gravity wave dynamics and effects in the middle atmosphere. *Rev. Geophys., 41(1),* 1-68, doi:10.1029/2001RG000106

Gelaro, R., McCarty, W., Suárez, M. J., Todling, R., Molod, A., Takacs, L., and Wargan, K. (2017), The modern-era retrospective analysis for research and applications, version 2 (MERRA-2). *J. Climate, 30(14),* 5419-5454.

Heale, C. J., and J. B. Snively (2015), Gravity wave propagation through a vertically and horizontally inhomogeneous background wind, *J. Geophys. Res. Atmos., 120*, 5931–5950, doi:10.1002/ 2015JD023505.

Hecht, J. H., R. L. Walterscheid, M. Hickey, and S. Franke (2001), Climatology and modeling of quasi-monochromatic atmospheric gravity waves observed over Urbana, Illinois, *J. Geophys. Res., 106(D6)*, 5181–5196.

Isler, J. R., M. J. Taylor, and D. C. Fritts (1997), Observational evidence of wave ducting and evanescence in the mesosphere, *J. Geophys. Res., 102*, 26,301–26,313.

Kam, Hosik (2016), Analysis of mesospheric gravity waves observed by an All-sky airglow camera at King Sejong Station, Antarctica, Master's thesis, Chungnam National University.

Kam, Hosik, Young-Sil Kwak, Yong Ha Kim, Tae-Yong Yang, Jaewook Lee, Jeongheon Kim, Ji-Hye Baek, Sunghwan Choi (2021), *J. Astron. Space Sci.*, in press.

https://doi.org/10.5194/angeo-2021-65
Preprint. Discussion started: 10 November 2021

Annales Geophysicae
Discussions

Kim, S-Y. and Chun H. Y. (2010), Stratospheric Gravity Waves Generated by Typhoon Saomai (2006): Numerical Modeling in a Moving Frame Following the Typhoon, *J. Atmos. Sci*., 67, 3617-3636.

Kim, Y. H., Lee, C. S., Chung, J. K., Kim, J. H., and Chun, H. Y. (2010), Seasonal variations of mesospheric gravity waves observed with an airglow all-sky camera at Mt. Bohyun, Korea (36 N). *J. Astron. Space Sci.*, *27*(3), 181-188.

Lindzen, R. S. (1981), Turbulence and stress owing to gravity wave and tidal breakdown. *J. Geophys. Res. Oceans.*, *86(C10)*, 9707-9714, doi:10. 1029/JC086iC10p09707

Nakamura, T., Higashikawa, A., Tsuda, T., and Matsushita, Y. (1999), Seasonal variations of gravity wave structures in OH airglow with a CCD imager at Shigaraki. *Earth, planets and space*, *51(7-8)*, 897-906.

Nappo, C.J. (2002). An Introduction to Atmospheric Gravity Waves. Academic Press, San Diego.

Nielsen, K., M. J. Taylor, R. E. Hibbins, M. J. Jarvis, and J. M. Russell III (2012), On the nature of short-period mesospheric gravity wave propagation over Halley, Antarctica, *J. Geophys. Res.*, *117*, D05124, doi:10.1029/2011JD016261.

Pautet, P., M. J. Taylor, A. Z. Liu, and G. R. Swenson (2005), Climatology of shot-period gravity waves observed over Northern Australia during the Darwin Area Wave Experiment (DAWEX) and their dominant source regions, *J. Geophys. Res.*, *110*, D03S90, doi:10.1029/2004JD004954.

Suzuki, S., K. Shiokawa, Y. Otsuka, S. Kawamura, and Y. Murayama (2013), Evidence of gravity wave ducting in the mesopause region from airglow network observations, *Geophys. Res. Lett.*, *40*, 601–605, doi:10.1029/2012GL054605.

Swenson, G. R., M. J. Alexander, and R. Haque (2000), Dispersion imposed limits on atmospheric gravity waves in the mesosphere: Observations form OH airglow, Geophys. Res. Lett., 27(6), 875–878.

Takeo, D., Shiokawa, K., Fujinami, H., Otsuka, Y., Matsuda, T. S., Ejiri, M. K., and Yamamoto, M. (2017). Sixteen year variation of horizontal phase velocity and propagation direction of mesospheric and thermospheric waves in airglow images at Shigaraki, Japan. *J. Geophys. Res.: Space Physics*, 122(8), 8770-8780.

Tang, J., Kamalabadi, F., Franke, S. J., Liu, A. Z. and Swenson, G. R. (2005). Estimation of

https://doi.org/10.5194/angeo-2021-65
Preprint. Discussion started: 10 November 2021

gravity wave momentum flux with spectroscopic imaging. *IEEE transactions on geoscience and remote sensing*, *43*(1), 103.

Taylor, M. J., Ryan, E. H., Tuan, T. F., and Edwards, R. (1993). Evidence of preferential directions for gravity wave propagation due to wind filtering in the middle atmosphere. *J. Geophy. Res. Atm.*, 98, 6047-6057. http://doi.org/10.1029/92JA02604.

Taylor, M. J., W. R. Pendleton Jr., S. Clark, H. Takahashi, D. Gobbi, and R. A. Goldberg (1997), Image measurements of short-period gravity waves at equatorial latitudes, J. Geophys. Res., 102, 26,283.

Vargas, F., G. Swenson, A. Liu, and D. Gobbi (2007), O(1S), OH, and O2(b) airglow layer perturbations due to AGWs andtheir implied effects on the atmosphere, *J. Geophys. Res.*, *112*, D14102, doi:10.1029/2006JD007642.

Walterscheid, R., J. Hecht, R. Vincent, I. Reid, J. Woithe, and M. Hickey (1999), Analysis and interpretation of airglow and radar observations of quasi-monochromatic gravity waves in the upper mesosphere and lower thermosphere over Adelaide, Australia (35°S, 138°E), *J. Atmos. Sol. Terr. Phys.*, *61(6)*, 461–478, doi:10.1016/S1364-6826(99)00002-4.

Yang, T.Y., Kwak,Y.-S., Kim, Y.H. (2015), Statistical comparison of gravity wave characteristics obtained from airglow all-sky observation at Mt. Bohyun, Korea and Shigaraki, Japan, *J. Astron. Space Sci.*, 32(4), 327-333.

https://doi.org/10.5194/angeo-2021-65
Preprint. Discussion started: 10 November 2021

Annales Geophysicae
Discussions

Figures

Figure 1 (a) an all-sky image with the OI 557.7 nm filter and (b) an image after star removal and coordinate transformation. The image was observed at 15:32:33 UT on May 26,2017.

Figure 2. (a) A time-difference image (TD image) obtained by taking a subtraction between two successive images, (b) an image after large-scale modulation removed from (a) by applying 2-D bandpass filtering.

Figure 3. The parameters of the observed waves in the OI 557.7 airglow layer from 2017-2019, (a) wavelength, (b) phase velocity, (c) period, and (d) propagation direction. Colors of blue, green, and orange correspond to each year of 2017-1019, respectively.

Figures 4. Propagation vectors (left) and the occurrences (right) of observed waves in the OI airglow over the three years from 2017 to 2019. (a) Spring, (b) Summer, (c) Fall and (d) Winter. The number on the arc lines indicate (left) the phase velocity and (right) occurrences in each radial direction. Wave propagation directions are divided into eight regions by a clockwise azimuth angle of 45° from -22.5° to 315°, corresponding to the north (N), northeast (NE), east (E), southeast (SE), etc. In fall, both equipment problem and poor weather resulted in particularly the small number of observations comparing to other seasons.

Figure 5. Seasonal distributions of observed (yellow) and intrinsic (green) wave parameters. Each row represents (a) Spring, (b) Summer, (c) Fall, and (d) Winter. Observed gravity waves are in total 150 events from April, 2017 to December, 2019, while intrinsic wave parameters were derived for 111 events when the wind data were available from the nearly co-located meter radar.

Figure 6. Examples of vertical propagation characteristics evaluated by vertical wave number squared, m^2, and the relation with horizontal wind. (left) the background wind in the direction of the gravity wave propagation and (right) the profile of m^2. (a) freely propagating, (b) Doppler ducted as encompassed by negative m^2, (c) evanescent based on negative m^2 at 90-97 km. Each title noted with the applied gravity wave occurring time, date and season. In addition, c and φ indicate the phase speed and azimuth angle of the horizontal propagation, respectively.

https://doi.org/10.5194/angeo-2021-65
Preprint. Discussion started: 10 November 2021

Annales Geophysicae Discussions
Open Access

Figures

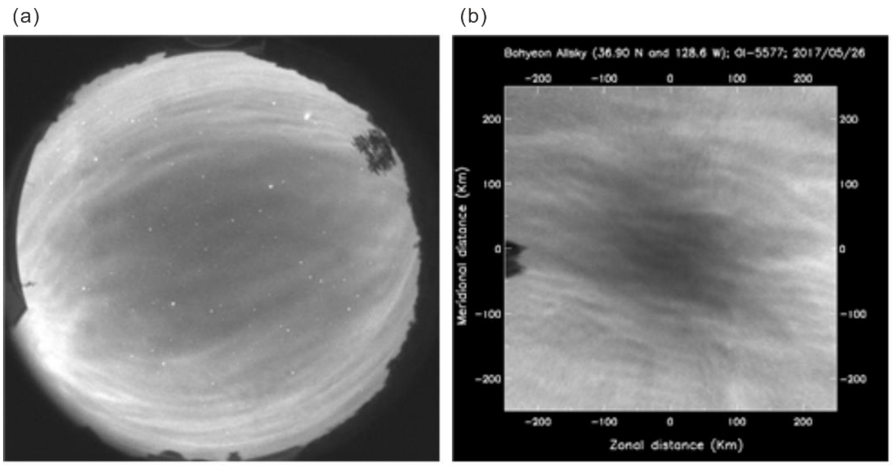

Figure 1.

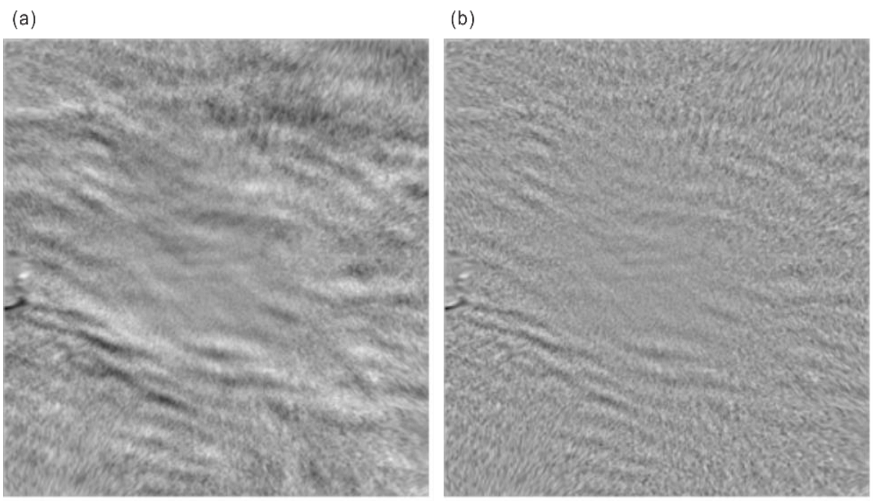

Figure 2.

https://doi.org/10.5194/angeo-2021-65
Preprint. Discussion started: 10 November 2021

Annales Geophysicae Discussions
Open Access
EGU

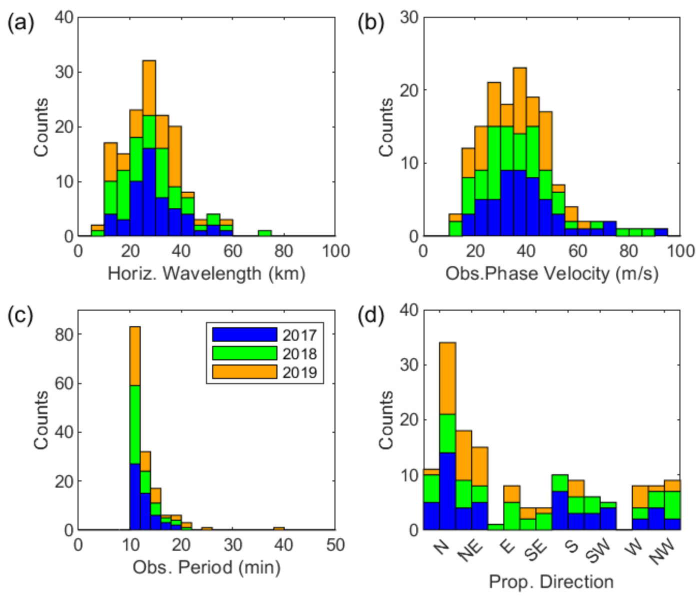

505

506 Figure 3.

https://doi.org/10.5194/angeo-2021-65
Preprint. Discussion started: 10 November 2021

Annales Geophysicae Discussions

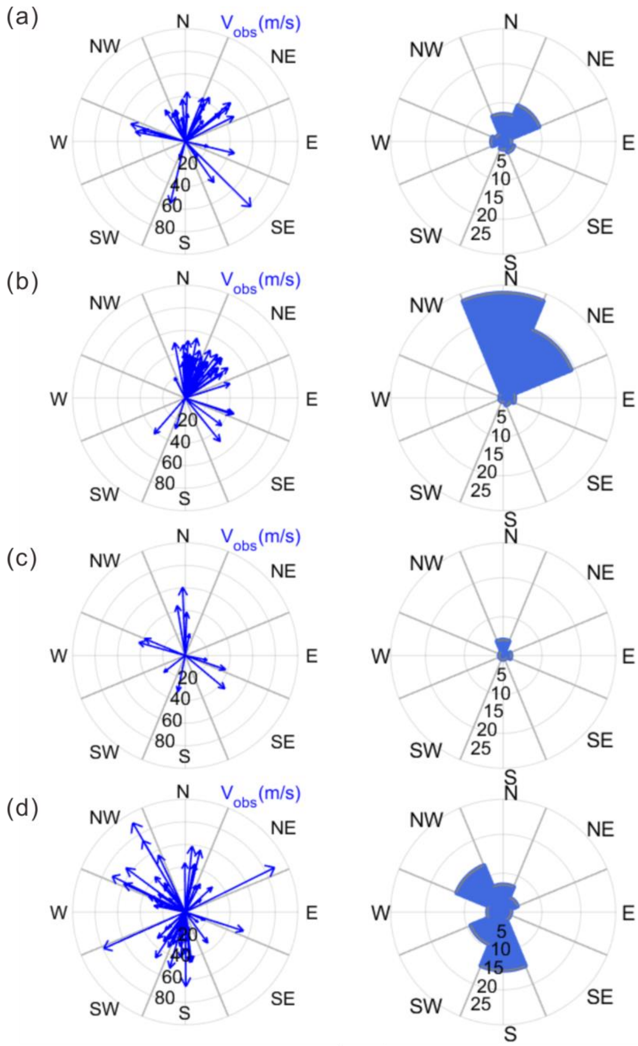

Figures 4.

https://doi.org/10.5194/angeo-2021-65
Preprint. Discussion started: 10 November 2021

Annales Geophysicae
Discussions
Open Access

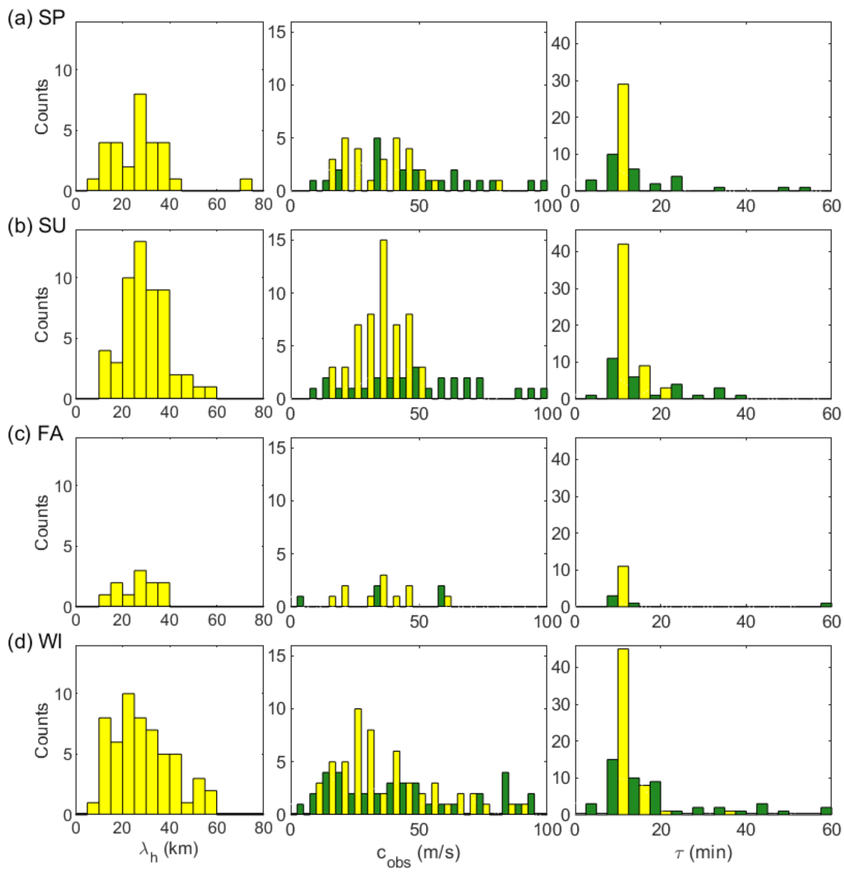

509

510 Figure 5.

511

https://doi.org/10.5194/angeo-2021-65
Preprint. Discussion started: 10 November 2021

Annales Geophysicae
Discussions
Open Access

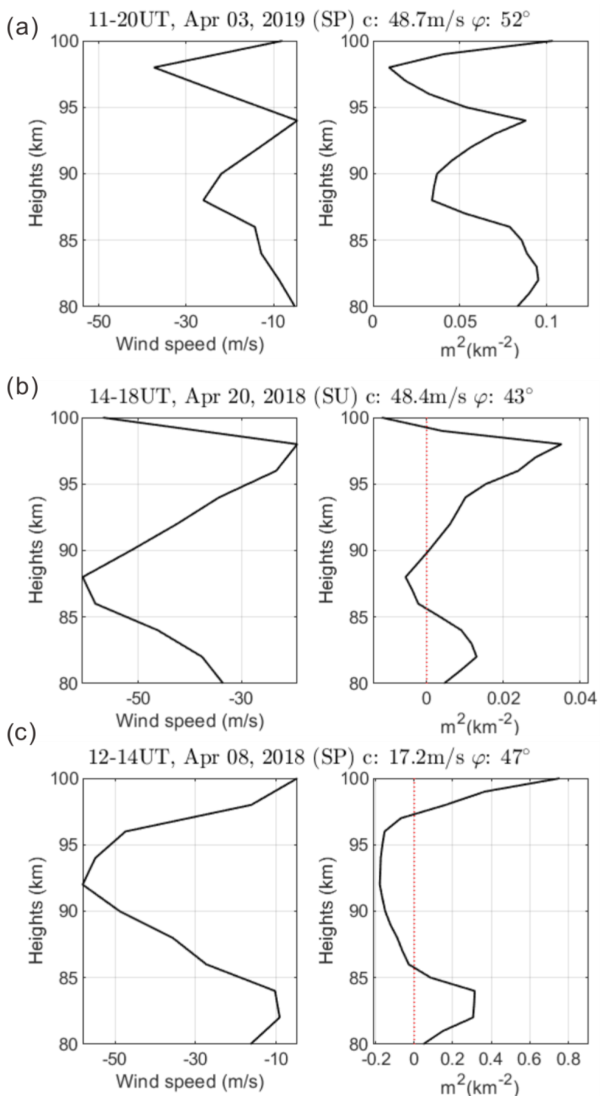

Figure 6.

https://doi.org/10.5194/angeo-2021-65
Preprint. Discussion started: 10 November 2021

Annales Geophysicae Discussions
Open Access

Table 1. Seasonal median values and interquartile ranges (IQR) of wave parameters (observed horizontal wavelength (λ_{obs}), observed phase speed (c_{obs}) and observed period (τ_{obs}) observed at Mt. Bohyun for 2017-2019.

Seasons	Parameters	λ_{obs} (km)	c_{obs} (m/s)	τ_{obs} (min)
Spring	Median	26.2	38.0	11.8
	IQR	18.0-31.4	24.8- 45.2	10.9- 13.6
Summer	Median	29.0	37.1	12.5
	IQR	23.7- 36.1	30.5- 42.1	11.3- 14.4
Fall	Median	25.7	38.7	11.7
	IQR	18.1-34.4	24.2- 45.1	10.7- 12.6
Winter	Median	27.5	32.7	11.5
	IQR	19.4-35.8	25.1- 46.7	10.8- 14.2

Table 2. Vertical propagation nature of gravity wave at Mt. Bohyun for 2017-2019.

	Spring (%)	Summer (%)	Fall (%)	Winter (%)
Freely Propagating	65	82	60	76
Ducting	0	7	20	4
Partial Ducting	28	11	20	20
Evanescent	7	0	0	0
Total (no. events)	29	28	5	49